Proceedings of the 21st ICSMGE, Vienna, Austria, 14 – 19 June 2026. Pistrol, Adam & Schweiger (eds.)
Published by: ÖGG, Austrian Society for Geomechanics, Salzburg, Austria, ISBN 978-3-9503898-4-5
https://doi.org/10.53243/ICSMGE2026-1844

Design and calibration of centrifuge tests to advance the understanding of tunnel response to driven piles

Lu Hai, Asaad Faramarzi, Nicole Metje
School of Engineering, University of Birmingham, Birmingham, United Kingdom, lxh224@student.bham.ac.uk

ABSTRACT: The development of cities involves construction activities many of which include installation of driven pile foundations. With increasing densification of cities and expansion of underground metro networks, new pile foundations may influence existing tunnels in their vicinity. However, the response of existing tunnels with segmental lining due to adjacent pile constructions has not been fully understood. This study presents the design, calibration, and preparation of a series of small centrifuge model tests intended to investigate the interaction between a tunnel and a driven pile installation in sandy soil. A soil pluviation technique was used to prepare the sand in the test cradle. The model tunnel lining, fabricated from aluminium alloy, incorporated grooves to simulate joint behaviour based on equivalent bending stiffness to replicate prototype conditions of a segmentally lined tunnel. A driven pile was made from steel and simplified as a sheet pile based on equivalent soil displacement. Instrumentation included six half-bridge strain gauges to capture tunnel lining behaviours, two load cells to record vertical earth pressures, and a Linear Variable Displacement Transformer (LVDT) to measure vertical ground surface movement. All instruments underwent rigorous calibration to ensure reliable interpretation of centrifuge test results. The calibration established voltage response relationships for all the sensors. Coefficients of determination exceeded 0.99 in all cases, indicating excellent linearity of the calibration relationships. This study established a validated experimental framework for future centrifuge investigations into the evaluation of the serviceability of an existing tunnel during pile installation, offering valuable data for urban construction practices.

KEYWORDS: Driven pile construction, tunnel, centrifuge tests, physical experiments, calibration

1 INTRODUCTION

Rapid urbanisation and population growth require more space in cities, not just above ground, but also below ground (Bélanger, 2007; Garrett, 2016) for foundations, utilities and tunnels. Ongoing expansion plans in many big cities e.g. (Greater London Authority, 2021) will exaggerate the problems of space and potentially lead to conflicts. Because of such plans, there will be more construction, like high-rise buildings, highways and bridges. In poor ground conditions, pile foundations are widely used to support these structures. Static-driven piles are getting popular due to low noise, high efficiency and safety (Liu et al. 2019). These pile foundations may increasingly occur close to existing tunnels. As reported in Liu et al. (2019), with a minimum clearance of 12.9 m between the existing tunnel equipped with segmental lining and the driven piles, the maximum horizontal displacement of the tunnel structure reached 23.7 mm, along with water leakage through the joints. Therefore, a more detailed understanding of the interaction between pile installation and existing tunnels is essential to support sustainable urban development.

In response to this need, several studies have been conducted over recent years to investigate the effects of pile construction on existing tunnels. Standing & Leung (2005) extended the photoelasticity technique to visualise stress paths in soil during pile driving near tunnels. The tests showed that the tunnel response weakened as the pile offset increased, and beyond one tunnel diameter, the influence became negligible. However, the method was qualitative, making it difficult to derive precise stress values. Salim & Lafta (2017, 2020) performed 1 g small-scale model tests in sand-filled steel tanks, with cast tunnel lining and piles. Displacement transducers and pressure cells recorded deformations and earth pressure. Results showed that the tunnel crown and invert experienced the highest stress concentrations, which reduced substantially with increasing pile offset and higher soil density, attributed to soil arching effects. He et al. (2020) proposed a calculation method based on cavity expansion theory to estimate horizontal tunnel displacements, incorporating pile group and blocking effects. Qin et al. (2013) simulated pile–tunnel interaction using FLAC3D, modelling both borehole expansion and shaft friction mobilisation. Their results, validated against analytical solutions, showed significant tunnel deformation, bending, and axial forces at small pile–tunnel distances, with a maximum settlement of 11.55 mm for a 20 m driven pile. Ding & Zhang (2019) applied PLAXIS 3D to study metro tunnel adjacent to a pile construction, finding the maximum tunnel deformation when piles were laterally adjacent, with the tunnel cross-section distorted into an oblique oval shape and an influence zone extending to ±20 m along the tunnel. Fall et al. (2021) used advanced finite element modelling with arbitrary Lagrangian–Eulerian (ALE) adaptive meshing and element deletion to capture large deformations and pile–soil interaction in detail. Their results showed how different tunnel depths relative to the pile length affected the displacement and stress distributions, providing insights into the spatial extent of influence.

Despite these contributions, gaps remain, particularly in accurately modelling segmental linings, considering scale effects in 1 g physical tests, and capturing joint behaviour in tunnels. To address these, the present study aims to design and conduct centrifuge model tests on tunnels with segmental lining, subject to adjacent pile loading in sandy soils. The analysis focuses on the deformation of the tunnel lining, earth pressure changes and soil movement, to provide improved understanding of soil–pile–tunnel interaction.

2 METHODOLOGY

The scaled physical tests in this study will be conducted using the beam-type geotechnical centrifuge equipped with multiple data acquisition channels at the National Buried Infrastructure Facility (NBIF). The machine has an effective radius of 0.66 m and a maximum acceleration capacity of 300 g. The maximum payload at each end of the beam is 90 kN.

The cradle used in the centrifuge tests consists of a rigid cuboidal frame constructed from high-tensile aluminium alloy, designed to withstand high g-forces. Clear Perspex is installed at both the front and back faces of the cradle, allowing visual observation of the soil and structural deformations during testing. The internal dimensions of the cradle are 0.3 m in length, 0.1 m in width, and 0.18 m in height.

To avoid boundary effects or ensure scaling compatibility, the centrifuge tests will be conducted at a centrifugal acceleration of 85 g. According to the scaling laws by Muir

Wood (2004), the dimensions of the model correspond to 25.5 m in length, 8.5 m in width and 15.3 m in height at prototype scale.

2.1 *Model tunnel*

The tunnel prototype in this study is adopted from recent work by Zhai et al. (2023). The key parameters of the prototype tunnel lining are summarised in Table 1.

Table 1. Dimension of the lining

Component		Unit	Value
segment	outer diameter (D)	m	6.2
	inner diameter (D_i)	m	5.5
	width (W)	m	1.2
bolt	diameter (d_b)	m	0.015
	Length (l)	m	0.485

The prototype tunnel segments and bolts are made of concrete and steel, respectively, with elastic moduli and Poisson's ratios of 30 GPa and 0.25 for concrete, and 206 GPa and 0.3 for steel. However, concrete is not suitable for use in the centrifuge model due to its relatively large aggregate size, which violates the particle size scaling requirements. The tunnel lining instead is represented by an aluminium alloy tube with a Young's modulus of 70 GPa and Poisson's ratio of 0.34. Given that the lining thickness is significantly smaller than the tunnel diameter, the required model thickness is determined using the scaling relationship proposed by Fang et al. (2022).

$$E_p I_p / E_m I_m = N \quad (1)$$

where E is the Young's modulus, I is the moment of inertia and N is a scale factor. The subscript m denotes model and p denotes prototype. Based on this scaling approach, the outer diameter of the model tunnel is 73 mm, with a thickness of 1.8 mm. Rectangular grooves were introduced to replicate the joints in the tunnel lining. The longitudinal joint grooves were designed using the principle of equivalent bending stiffness (Li et al. 2023), with dimensions of 2 mm in width and 0.8 mm in depth. The circumferential joints are represented by grooves of the same dimensions to maintain consistency.

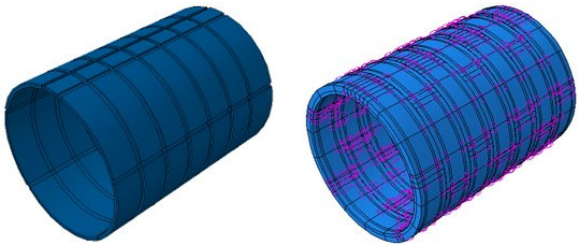

(a) (b)

Figure 1. Numerical model to determine the groove for the circumferential joints: (a) Model 1: tunnel lining with grooves; (b) Model 2: prototype tunnel lining (bolts are represented by springs)

To assess the validity of the simulated joints, two numerical models were developed to compare the longitudinal structural behaviour of the tunnel lining. The first model represents the centrifuge-scale segmental tunnel, incorporating the detailed geometry and groove-based joints (Figure 1 (a)). The second model represents the full-scale prototype tunnel, comprising seven segmental rings, where bolts were modelled as spring elements (Zhai et al. 2023) to simulate the mechanical response at the circumferential joints (Figure 1 (b)). The tensile stiffness of the spring elements was calculated using Equation (2), ensuring an accurate representation of joint behaviour in the prototype.

$$K_s = EA/l \quad (2)$$

Where K_s is the tensile stiffness of the spring. E is the elastic modulus of the bolt; A is the cross-sectional area of the bolt and l is the length of the bolt.

To verify the displacement behaviour of the tunnel lining, a uniform pressure of 120–200 kPa was applied to the model, representing the scaled earth pressure during centrifuge testing. Figure 2 shows that both numerical models exhibit similar settlement trends, indicating that the model tunnel with grooves to simulate joints adequately captures the mechanical behaviour of segmental tunnel linings. This confirms the validity of the joint representation used in the scaled model.

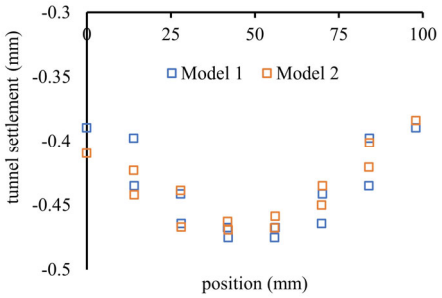

Figure 2. Comparison between the simulation methods in terms of vertical displacement of the lining

Finally, the assembled model tunnel, incorporating the machined joint grooves and scaled geometry, is shown in Figure 3.

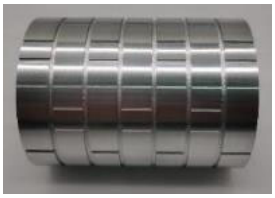

Figure 3. Model tunnel

The model tunnel is positioned inside the cradle with a horizontal offset of 1.5 D from the side boundary and a vertical offset of 1D from the bottom, to minimise boundary effects and ensure uniform stress conditions in the central region. In the plane strain configuration, the tunnel is placed in direct contact with both front and back Perspex windows of the model box, ensuring that the observed deformation field accurately represents the soil–structure interaction as shown in Figure 4.

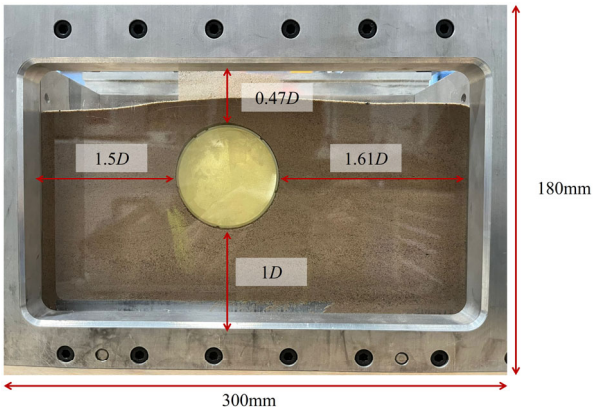

Figure 4. The position of the model tunnel inside the cradle

To prevent sand ingress during testing, both ends of the tunnel are sealed with a thin, flexible plastic membrane conforming closely to the tunnel profile. A thin layer of grease is applied at the membrane–Perspex interface to reduce friction and allow relative sliding during loading, thereby minimising artificial

restraint and distortion of the soil displacement field. The tunnel is carefully aligned and fixed in position, and any excess grease on the Perspex is cleaned to preserve optical clarity for Particle image velocimetry (PIV) analysis.

2.2 *Pile modelling and installation*

In the prototype configuration, the row of circular piles (1 m diameter, 4 m spacing) has been idealised as a continuous sheet pile, preserving the equivalent volume of displaced soil per unit width. Assuming the same elastic modulus, the equivalent sheet pile thickness was determined using Equation (3).

$$\left(\pi d_p^2/4s\right) = t_m \tag{3}$$

Where d_p is the diameter of an individual prototype pile, and s is the spacing between adjacent piles in the row. t_m is the equivalent sheet pile thickness. The calculated equivalent thickness of the sheet pile is 0.196 m.

This was then scaled down for the centrifuge model, resulting in a sheet pile thickness of 2.3 mm made from steel. The steel sheet pile used in the tests is 130 mm long, with a penetration depth of 90 mm into the model ground. To ensure stable and accurate installation, two bolts are attached to the pile head and fixed to the linear actuator, ensuring rigid connection and vertical insertion without rotation. A schematic of the sheet pile configuration is provided in Figure 5 (a).

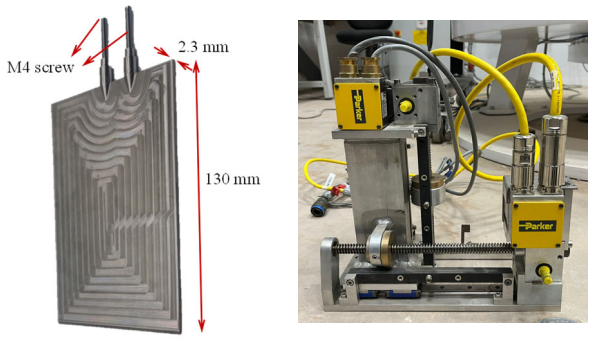

(a) (b)

Figure 5. Pile installation in the physical tests: (a) sheet pile; (b) linear actuator

The pile penetration process will be executed at a speed of 0.1 mm/s using a dual-axis electric linear actuator, as illustrated in Figure 5 (b). Displacement feedback from the actuator will be logged and synchronised with the sensor data acquisition for post-processing analysis.

2.3 *Sand*

The sand used in the centrifuge tests is a clean silica sand (SANSIL/L: Certified Leisure Sand Loose, Long Rake Spar Ltd., UK), chosen for its high silica content, consistent grading, and rounded to sub-angular particle shape, making it well-suited for controlled laboratory experiments.

2.3.1 *Properties of the sand*

As shown in Figure 6, the sand exhibits a coefficient of uniformity (C_u) of 2.00 and a coefficient of curvature (C_c) of 1.13, indicating a poorly graded, fine- to medium-grained material. The maximum and minimum dry densities were determined using ASTM D4253-00 and ASTM D4254-00, yielding values of 1.721 g/cm³ and 1.595 g/cm³, respectively. A peak internal friction angle of approximately 30.4° was determined using direct shear tests conducted under drained conditions, indicative of a medium-dense behaviour typical for silica sands with rounded grains.

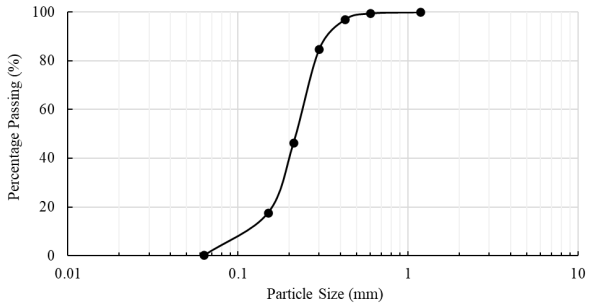

Figure 6. Soil particle size distribution

2.3.2 *Soil rain into the cradle*

The dry pluviation method was employed to prepare the sand bed within the test cradle. This was achieved using the calibrated pluviation station at NBIF (Figure 7), which ensured consistent deposition and controlled density. Sand was poured from a sand box through a fixed nozzle, allowing grains to fall under gravity onto the model surface. The drop height and flow rate were carefully adjusted to maintain uniform relative density and minimise dispersion.

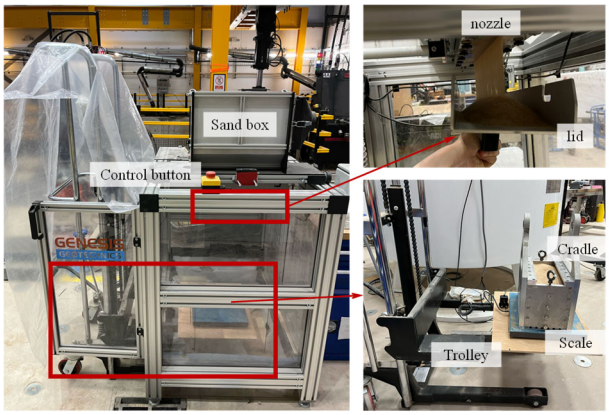

Figure 7. Setup for the pluviation

The cradle was placed on a digital scale to monitor the mass of sand deposited during filling. Sand was pluviated into the cradle in five layers of thickness 36.5, 36.5, 36.5, 36.5, and 34 mm (corresponding to one tunnel radius for the first four layers), ensuring uniform density throughout the model depth. The drop height was kept constant for all layers by adjusting the height of the trolley holding the sand box.

2.3.3 *Relative density determination*

The initial nozzle–cradle distance was set to 653 mm, with a nozzle opening of 1.8 mm. Under these conditions (without a tunnel), the measured relative density of the sand was 59.5%, corresponding to a medium-dense state (Table 2).

Table 2. Pluviation results for the case without model tunnel

Variables	Volume	Weight sand	Density	Dr
Unit	m^3	kg	(kg/m^3)	-
Layer 0	0	0	0	0.00%
Layer 1	0.00108	1.82	1685	62.75%
Layer 2	0.00112	1.88	1679	58.33%
Layer 3	0.00108	1.82	1685	62.75%
Layer 4	0.00106	1.78	1679	58.78%
Layer 5	0.00104	1.74	1673	54.62%
Sum	0.00538	9.04	1680	59.48%

2.4 *PIV technique*

The PIV technique will be used to capture the soil deformation field during testing, based on digital image analysis of surface texture patterns between consecutive images (White et al.

2003). A high-resolution industrial camera will be positioned on the cradle, in the centrifuge and faced to the Perspex to provide a clear, unobstructed view of the model face. Images are recorded at fixed intervals throughout the test.

Uniform and diffuse illumination will be achieved using a custom-enclosed lighting system fitted with a white Perspex diffuser. This setup minimises glare and shadows, ensuring consistent lighting conditions necessary for accurate image correlation.

To enhance the surface texture and improve PIV tracking accuracy, approximately 15% of the sand grains (by weight) were dyed black using Daler–Rowney Kandahar ink. After drying, the dyed particles were thoroughly mixed with the natural sand to generate a random speckled pattern across the model surface, suitable for high-fidelity image correlation.

Image capture will be managed using IDS Peak Cockpit software, which provides live preview capabilities and allows for precise adjustment of imaging parameters such as exposure time, frame rate and resolution.

3 INSTRUMENTATION

To monitor the tunnel and soil response during pile penetration, a comprehensive instrumentation system will be deployed to measure earth pressures, structural strains, and surface displacements as shown in Figure 8. The system comprises:

- Load cells, positioned at the tunnel invert level, to measure horizontal and vertical earth pressures;
- Strain gauges, installed on the tunnel lining to capture bending and axial strains during loading;
- An LVDT, placed at the ground surface, to record vertical surface settlements.

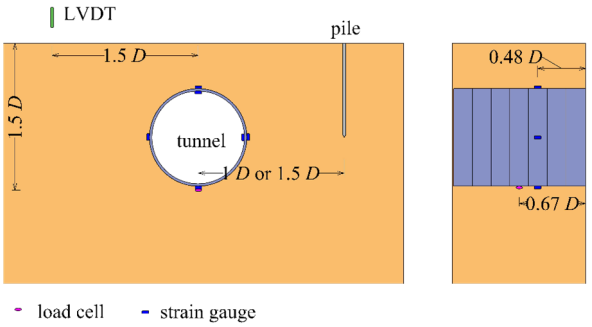

Figure 8. Positions of strain gauges on the model tunnel

All analogue signals were digitised using an MCC 128 DAQ HAT, interfaced with a Raspberry Pi, which serves as the central data logger. To ensure signal quality and reliability, each strain gauge and load cell output was first routed through an AD620 instrumentation amplifier module, which amplifies and conditions the signals prior to data acquisition.

3.1 *Strain gauge*

The induced strain change in the model tunnel is measured by strain gauges of model KFH-3-350-C1-11L1M2R (with 350 Ω resistance). The strain gauges were arranged in a half-bridge configuration to improve sensitivity and thermal stability, as shown in Figure 9. All strain gauges were orientated circumferentially around the tunnel lining to capture bending and axial strains resulting from soil–structure interaction during pile penetration. Strain measurements were taken on both sides of the crown, the left side (facing the adjacent pile), the outer face of the invert, and the right side (opposite the pile). Strain gauges were securely bonded to the tunnel lining using high strength adhesive, with a thin layer of silicone sealant applied over each gauge to protect against abrasion from the sand during testing.

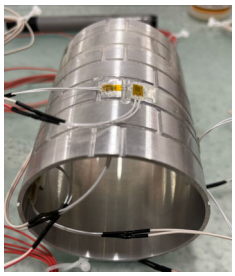

Figure 9. The arrangement of strain gauge on the model tunnel

Following installation, the strain gauges were calibrated to establish a reliable relationship between output voltage and actual strain in the tunnel lining. The gauge signals were amplified using AD620 amplifiers to ensure sufficient resolution and signal stability for data acquisition. The calibration setup is shown in Figure 10 (a). To prevent lateral movement or rolling during loading, the model tunnel was seated in a precision-cut groove on a base plate. Known vertical loads were incrementally applied by placing calibrated weight plates on top of the tunnel to induce controlled strains. To capture both tensile and compressive responses, the tunnel was tested in two orientations: first, with the invert resting on the base plate to induce compression at the crown, and then, with the springline seated, allowing for strain measurements at the crown, invert, and springline under different bending conditions. Theoretical strain distributions were computed using a numerical simulation of the calibration setup, shown in Figure 10 (b). These results will provide reference strain values for comparison with experimental measurements.

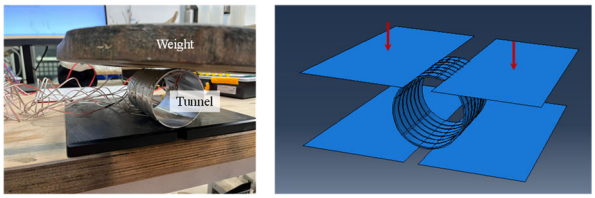

(a) (b)

Figure 10. Numerical modelling for the strain calibration

A linear regression analysis was performed for each of the six half-bridge strain gauges to establish the relationship between measured output voltage and corresponding mechanical strain. The resulting calibration equations were expressed in the form: $V_{out} = \mathrm{A} * \varepsilon + \mathrm{B}$. The V_{out} is the amplified voltage output in units of V and ε is the strain. The amplification, A (V/strain) and B (V) for each strain gauge are summarised in Table 3.

Table 3. Summary of the calibration results of strain gauges

Position	Amplification	Calibration equation		
		A	B	R^2
Crown outer face	287	-666.48	0.0052	0.998
Crown inner face	239	-1981.00	-0.0190	0.994
Invert outer face	187	-655.16	-0.0020	0.999
Left outer face	245	-1240.30	-0.1059	0.992
Left inner face	225	-977.58	-0.0133	0.996
Right outer face	178	-682.86	-0.0440	0.996

The coefficient of determination R^2 for all regression fits exceeded 0.99, indicating excellent calibration linearity

3.2 *Linear Variable Differential Transformer*

A Linear Variable Differential Transformer (LVDT) will be employed to measure vertical ground surface displacements during pile installation, allowing direct comparison with

displacement fields captured via the PIV technique. The LVDT employed has a calibrated measurement range of ±5 mm and a sensitivity of 53.46 mV/V/mm, operating under a 10 V DC excitation.

To ensure accuracy, the LVDT was calibrated by determining a precise voltage–displacement relationship. As shown in Figure 11 (a), the LVDT was mounted in a vertical orientation, with its moveable core in contact with a precision micrometre screw gauge. Controlled vertical displacements were applied incrementally using a micrometre, and the corresponding voltage output was recorded.

The calibration data is shown in Figure 11 (b). A linear regression analysis was conducted to establish the relationship between displacement and voltage output. The calibration yielded the following equation:

$$V_{out} = \mathrm{C} * Displacement + \mathrm{D} \quad (4)$$

V_{out} is the output voltage from the datalogger. C is 0.576 V/mm and D is 5.2685 V. With a coefficient of determination $R^2 = 0.9992$, it indicates good linearity.

Although slight non-linearity is observed at the extreme ends of the calibration range, the LVDT exhibits a strong linear response within the displacement interval of 6–14 mm. This range is selected as the effective operating window for the centrifuge tests to ensure both accuracy and stability of the displacement measurements. The calibrated voltage–displacement relationship (Equation (4)) is subsequently used to convert raw voltage signals into displacement values during post-processing.

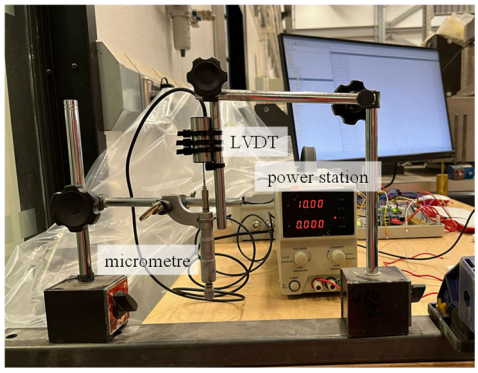

(a)

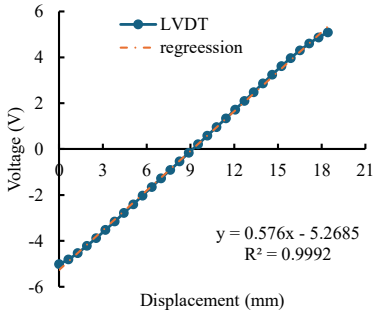

(b)

Figure 11. Calibration of LVDT: (a) calibration configuration of the LVDT; (b) the relationship between voltage and displacement

3.3 *Load cell*

To monitor vertical earth pressure within the sandy soil during pile penetration, three compression-type load cells (TE Connectivity FX29 series) will be embedded at the tunnel invert level, as shown in Figure 12. One load cell with a 250 N range and one with a 125 N range will be used, designated load cell 01 and load cell 02, respectively. The vertical earth pressure will be determined by dividing the measured load by the known cross-sectional area of each load cell.

Figure 12. FX29 compression load cell

Each load cell operates with a 5 V DC excitation and generates an analogue output signal of up to 100 mV, necessitating external amplification for signal clarity and compatibility with the data acquisition system. To ensure the output voltage is both discernible and within the measurable range, amplification factors of 12 and 25 were applied to load cell 01 and 02, respectively.

Calibration of the load cells was carried out using a controlled vertical loading setup, as shown in Figure 13. Known weights were applied incrementally to establish the relationship between applied load and output voltage, enabling accurate conversion of measured signals into pressure values during testing.

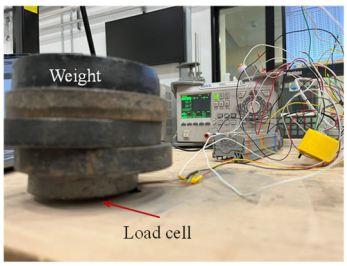

Figure 13. Calibration setup for load cells

Calibration results, presented in Figure 14 (a) and (b), demonstrate excellent linearity for both load cell types, with coefficients of determination R^2>0.99. The resulting calibration equations, which relate the applied load to the amplified voltage output V_{out}, are embedded within the data acquisition scripts. This enables real-time conversion of voltage signals into accurate force measurements throughout the testing process.

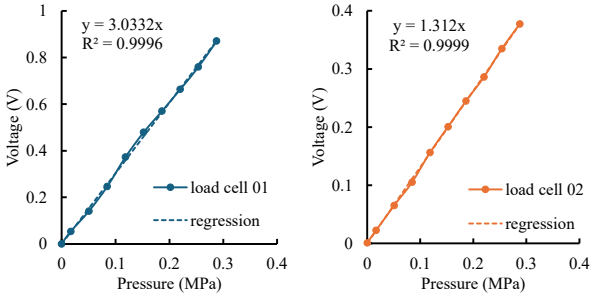

(a) (b)

Figure 14. Calibration results of load cell: (a) 01 and (b) 02

The linear regression analysis for load cell 01 and load cell 02 produced Equation (5) and (6):

$$V_{out} = \mathrm{E} * Pressure \quad (5)$$

$$V_{out} = \mathrm{F} * Pressure \quad (6)$$

V_{out} is the output voltage recorded by the data acquisition system, Pressure in MPa is the applied vertical force divided by the load cell area and E and F are constants with E = 3.0332 V/MPa and F = 1.3120 V/MPa. Both equations exhibited strong linearity, with coefficients of determination $R^2 > 0.99$ indicating excellent linearity of the calibration relationship.

4 PLANNED TEST SCENARIOS

A total of seven tests will be conducted, all with medium-dense sand. The test matrix is designed to investigate the soil–tunnel–pile interaction mechanisms under different configurations, while also assessing repeatability and the potential influence of sensor wiring.

Tests 1-1 and 1-2 will be performed under greenfield conditions, i.e., with pile installation in the absence of a tunnel. Test 1-2 will be a repeat of Test 1-1 to assess the repeatability of the results. In Test 1-1, the response of the soil to pile installation will be recorded using a camera and an LVDT, whereas in Test 1-2 only the LVDT will be used. Repeatability will be validated by comparing the output signals of the LVDT between the two tests.

Tests 2-1 and 2-2 will examine the influence of segmental joints in the tunnel lining, with the tunnel installed at a clearance of one tunnel diameter from the pile. Both tests will use a single load cell at the tunnel invert level to measure vertical earth pressure and an LVDT at the ground surface. A camera facing the Perspex will be mounted on the cradle to capture the soil movement.

Tests 3-1 and 3-2 are designed to investigate the influence of reduced clearance between the pile and tunnel. In these tests, the pile will be positioned only 0.5 tunnel diameters away from the tunnel, while all other instrumentation and setup remain the same as in Tests 2-1 and 2-2.

5 CONCLUSIONS

This paper presented the design methodology and calibration procedures for a small centrifuge model aimed to investigate the interaction between driven pile installation and existing segmentally lined tunnels in sandy soils. This will improve the understanding of the potential risks and deformation mechanisms of the tunnel associated with nearby pile construction in densely urban environments.

A comprehensive experimental methodology was designed, involving high-g centrifuge model tests. The physical model features a segmentally lined tunnel represented using an aluminium alloy tube with scaled groove joints, validated through comparative numerical simulations. Pile installation was modelled using a scaled steel sheet pile actuated by a programmable linear actuator, while soil displacements and tunnel responses are measured via a carefully integrated instrumentation system of strain gauges, load cells, LVDTs, and high-resolution PIV-based image analysis. All sensors have been carefully calibrated providing confidence in the results.

The test matrix plans to include seven planned experiments covering greenfield, existing tunnel, and pile–tunnel clearance effects, with repeat tests for validation. The experimental setup is designed to produce high-fidelity data for benchmarking and future numerical model calibration.

Once testing is complete, the framework developed in this study will enable detailed analysis of the soil deformation field, tunnel joints behaviour, and stress redistribution mechanisms induced by pile penetration. These findings will support the development of more reliable design guidelines and risk assessment frameworks for pile construction near existing tunnels in granular soils.

ACKNOWLEDGEMENTS

The corresponding author would like to acknowledge the China Scholarship Council (Grant Ref. 202207090016) for their support. This research was also supported by funding from the UK Engineering and Physical Sciences Research Council via its support for the UK Collaboratorium for Research on Infrastructure and Cities (UKCRIC, Grant Ref. EP/R017727) and specifically UKCRIC NBIF (Grant Ref. EP/P013635).

REFERENCE

Bélanger, P. 2007. Underground landscape: The urbanism and infrastructure of Toronto's downtown pedestrian network. *Tunnelling and Underground Space Technology*. 22(3):272–292. DOI: 10.1016/j.tust.2006.07.005.

BROADBENT. 2018. *OPERATING MANUAL (GT6/0.75 Geotechnical Beam Centrifuge)*.

Ding, Z. and Zhang, X. 2019. Numerical analysis of influence of pile foundation construction on adjacent metro tunnel. *Journal of Central South University (Science and Technology)*. 50(2):390–399.

Fall, M., Gao, Z. and Ndiaye, B.C. 2021. Safety evaluation of existing tunnel nearby driving pile using two different standards. *International Journal of Geomechanics*. 21(3):1–11. DOI: 10.1061/(asce)gm.1943-5622.0001948.

Fang, Q., Liu, X., Zeng, K., Zhang, X., Zhou, M. and Du, J. 2022. Centrifuge modelling of tunnelling below existing twin tunnels with different types of support. *Underground Space (China)*. 7(6):1125–1138. DOI: 10.1016/j.undsp.2022.02.007.

Garrett, B.L. 2016. Picturing urban subterranea: Embodied aesthetics of London's sewers. *Environment and Planning A*. 48(10):1948–1966. DOI: 10.1177/0308518X16652396.

Greater London Authority. 2021. *the spatial development strategy for Greater London*. London: Greater London Authority. Available: www.london.gov.uk.

He, L., Zhang, Y. and Ma, S. 2020. A study on the calculation method of horizontal displacement of adjacent tunnels caused by static pressure sinking piles. *Rock and Soil Mechanics2*. 41(11):3740-3747+3809.

Li, H., Li, X. and Liu, H. 2023. Deformation and failure mechanism of metro shield tunnel subjected to buried fault dislocation. *Engineering Failure Analysis*. 153(August):107551. DOI: 10.1016/j.engfailanal.2023.107551.

Liu, X., Sang, Y., Zhao, F., Shi, G. and Heng, Y. 2019. Evaluation of effects of static pile driving on existing metro tunnel structure. *Journal of Performance of Constructed Facilities*. 33(4):1–11. DOI: 10.1061/(asce)cf.1943-5509.0001309.

Muir Wood, D. 2004. *Geotechnical Modelling (1st ed.)*. London: CRC Press. DOI: https://doi.org/10.1201/9781315273556.

Qin, S., Zhou, Y. and Mo, L. 2013. Influences of driving pile on neighboring tunnel. *JOURNAL OF SHANGHAI UNIVERSITY (NATURAL SCIENCE*. 19(05):527–533.

Salim, N. and Lafta, S. 2017. The Impact of Driving and Loading Piles on Existing Tunnel. *Imperial Journal of Interdisciplinary Research*. 3(7):2454–1362. Available: http://www.onlinejournal.in.

Salim, N. and Lafta, S. 2020. Effect of a driven pile on an existing tunnel. *Journal of Engineering and Sustainable Development*. 24:94–109. DOI: 10.31272/jeasd.24.1.7.

Standing, J. and Leung, W. 2005. Investigating stresses around tunnels and piles using photo-elasticity techniques. In *Proc., 5th Int. Symp. on Geotechnical Aspects of Underground Construction in Soft Ground*. 171–177.

White, D.J., Take, W.A. and Bolton, M.D. 2003. Soil deformation measurement using particle image velocimetry (PIV) and photogrammetry. *Géotechnique*. 53(7):619–631. DOI: 10.1680/geot.2003.53.7.619.

Zhai, W., Zhang, D., Huang, H. and Chapman, D. 2023. Numerical investigation into the composite behaviour of over-deformed segmental tunnel linings strengthened by bonding steel plates. *Soils and Foundations*. 63(4):101335. DOI: 10.1016/j.sandf.2023.101335.